SIAM J. SCI. COMPUT.
Vol. 19, No. 4, pp. 1154–1168, July 1998

006

FINITE ELEMENT APPROXIMATION OF THE DIFFUSION OPERATOR ON TETRAHEDRA*

MARIO PUTTI† AND CHRISTIAN CORDES†

Abstract. Linear Galerkin finite element discretizations of the Laplace operator produce nonpositive stiffness coefficients for internal element edges of two-dimensional Delaunay triangulations. This property, also called the positive transmissibility (PT) condition, is a prerequisite for the existence of an M-matrix and ensures that nonphysical local extrema are not present in the solution. For tetrahedral elements, it has already been shown that the linear Galerkin approach does not in general satisfy the PT condition. We propose a modification of the three-dimensional Galerkin scheme that, if a Delaunay triangulation is used, satisfies the PT condition for internal edges and, if further conditions on the boundary are specified, yields an M-matrix. The proposed approach can also be extended to the general diffusion operator with nonconstant or anisotropic coefficients.

Key words. finite elements, Galerkin method, three-dimensional Delaunay triangulation

AMS subject classifications. 65N12, 65N30, 65N35

PII. S1064827595290711

1. Introduction.

Finite element schemes are commonly used in the solution of second-order partial differential equations (PDEs) arising from many practical applications such as, for example, heat transfer, groundwater flow and contamination, petroleum reservoir simulation, and Navier–Stokes equations. The discretization of the diffusion operator of the PDE is often carried out by means of the Galerkin approach. It is well known that the use of the Galerkin formulation on triangular elements with linear (C^0) basis functions leads, in some cases, to wrong solutions that do not satisfy the maximum principle (local extrema occur inside the domain) [9]. This problem has been linked with the fact that the system matrix resulting from the discretization is not an M-matrix [5]. The existence of an M-matrix implies that the so-called PT condition [14, 12] is satisfied. This fact guarantees that the discrete flux between two nodes is in the opposite direction of the dependent variable gradient.

For Laplace equation in two dimensions, a sufficient condition for nonpositive Galerkin off-diagonal stiffness coefficients is that the triangulation be made of acute or right-angled triangles [6]. In general it can be shown that if the triangulation is Delaunay, the linear Galerkin stiffness coefficient satisfies the PT condition for all nodal pairs representing internal element edges (edges not lying on the domain boundary) [5]. If, furthermore, no circumcenters of boundary elements lie outside the domain, then the PT condition is guaranteed over the entire domain. Under these hypotheses, and if at least one Dirichlet boundary condition is imposed, the linear Galerkin approach on triangles leads to an M-matrix.

In three space dimensions, tetrahedral elements are the natural extensions of triangles. However, it was shown in [9], via a counterexample, that the linear Galerkin approach for the Laplace operator does not always satisfy the PT condition even on

*Received by the editors August 22, 1995; accepted for publication (in revised form) August 19, 1996; published electronically April 16, 1998.
http://www.siam.org/journals/sisc/19-4/29071.html
†Dipartimento di Metodi e Modelli Matematici per le Scienze Applicate, University of Padua, via Belzoni 7, Padova, Italy (putti@dmsa.unipd.it, cordes@dmsa.unipd.it). The work of the first author was partially supported by EC contract AVI-73. The work of the second author was supported by EERO.

internal edges of a Delaunay mesh and thus cannot guarantee an M-matrix. The reason for this behavior can be better understood by looking at the physical interpretation of the stiffness coefficient. In both two and three dimensions, the linear Galerkin stiffness coefficient can be alternatively expressed as the flux of the basis function gradient across the boundary of a specific nodal control volume. We will prove that these control volumes, in a two-dimensional Delaunay triangulation, can be identified by the Voronoi mesh restricted to the domain of definition of the PDE and are characterized by having cell boundaries orthogonal to the element edges and vertices on the circumcenters of the triangles. In three dimensions, we will show that the Galerkin subdomains may be interpreted as control volumes having vertices not on the circumcenters but on the gravity centers of the tetrahedra. Thus, they cannot take the shape of Voronoi cells, except in regular tetrahedra, for which circumcenters and gravity centers coincide.

In this paper, we propose a modification of the Galerkin approach by defining the vertices of the control volumes as being the circumcenters and not the gravity centers [2, 3]. For the Laplace operator, we will prove that this approach, called orthogonal subdomain collocation (OSC), satisfies the PT condition for internal element edges of a three-dimensional Delaunay triangulation and, under suitable conditions on the boundary, yields an M-matrix.

In the next sections, we will use the following definitions and properties of Delaunay triangulations and Voronoi diagrams. A Delaunay triangulation in $\mathbb{R}^d$ is defined by the condition that the circumsphere of each triangle contains no other nodes in its interior [8]. Its dual is the Voronoi diagram, also called Voronoi mesh or set of Thiessen polyhedra [4], which can be defined as follows [13]: let P_i, $1 \leq i \leq n$, be a set of points in $\Omega \subset \mathbb{R}^d$, and let Ω be the convex hull of all the P_i. We assume that Ω coincides with the domain of definition of the diffusion equation. Denote by $H(P_i, P_j)$, $i \neq j$, the closed half space containing P_i, bounded by the bisecting hyperplane of the segment P_iP_j. The Voronoi cell (or Thiessen polyhedron), V_i, of P_i is defined as the intersection of all $H(P_i, P_j)$, $j \neq i$. The Voronoi mesh is then the set of all V_i, $1 \leq i \leq n$. In other words, the interior of the Voronoi cell $\overset{\circ}{V}_i$ is the set of points $s \in \mathbb{R}^d$ characterized by having a smaller distance from P_i than from any other point P_j. A Voronoi diagram satisfies the following properties [13, 1]:

(P1) $$\bigcup_{i=1}^{n} V_i = \mathbb{R}^d, \qquad \overset{\circ}{V}_i \bigcap \overset{\circ}{V}_j = \emptyset;$$

(P2) the Voronoi cell V_i of each point P_i takes the shape of a convex d-dimensional polyhedron; V_i is unbounded if P_i lies on $\partial\Omega$ (the boundary of Ω), bounded otherwise;

(P3) if P_iP_j is an edge of a Delaunay triangulation then the intersection of V_i and V_j is nonempty and takes the shape of a convex $(d-1)$-dimensional polyhedron, orthogonal to P_iP_j in the midpoint; this polyhedron is unbounded if P_iP_j lies on $\partial\Omega$, bounded otherwise;

(P4) the vertices of the Voronoi cells are the circumcenters of the Delaunay simplices.

An example of a two-dimensional Delaunay triangulation with the corresponding Voronoi cell V_j is shown in Figure 1. Note that the Thiessen polygons can be interpreted as nodal control volumes for a finite element mesh.

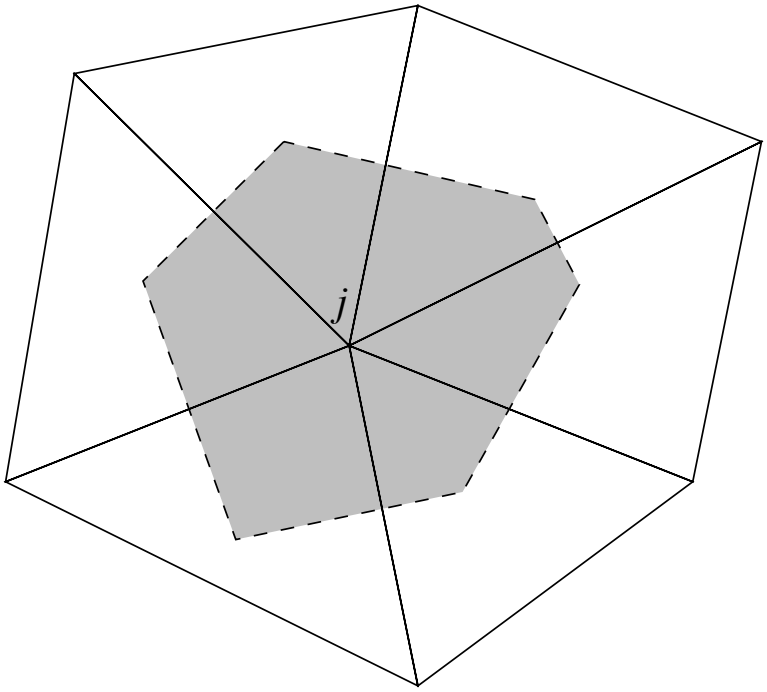

FIG. 1. *Two-dimensional Delaunay triangulation and corresponding Voronoi cell V_j (Thiessen polygon).*

In the next two sections we will focus on discretization schemes for the Laplace operator

$$\mathcal{L}u = \nabla \cdot \nabla\, u \tag{1}$$

considered as an element of a more general elliptic equation defined on a general convex domain Ω, with given boundary conditions on $\partial\Omega$. Extensions of the discretization methods for the general diffusion operator with a possibly nonconstant conductivity tensor D,

$$\mathcal{L}_1 u = \nabla \cdot D\nabla u \tag{2}$$

will be addressed in the last section.

2. Galerkin stiffness coefficients in two and three dimensions. The elemental Galerkin stiffness coefficient for Laplace equation (1) can be generally expressed as

$$s_{ij}^{e,G} = \int_e \nabla N_i \cdot \nabla N_j dA, \tag{3}$$

where N_i is the basis function and A is the area (volume) of element e. The global Galerkin stiffness coefficient is obtained by summation of $s_{ij}^{e,G}$ over all elements:

$$s_{ij} = \sum_e s_{ij}^{e,G}.$$

Denoting by L the number of nodes in element e, it is well known that the global stiffness coefficients satisfy the property [15]:

$$\sum_{j=1}^{L} s_{ij}^{e,G} = 0. \tag{4}$$

2.1. Two spatial dimensions. Let T be a triangle with vertices i, j, and k (Figure 2). Define the edge vector $\boldsymbol{r}_{ij}$ as the vector connecting node i with node j, oriented from i to j. Let $\boldsymbol{n}_j$ be the unit vector normal to edge $\boldsymbol{r}_{ik}$, opposite to node j, and pointing toward j.

By definition, N_j is a linear function with value one on node j and zero on nodes i and k. The gradient of N_j is therefore a constant vector orthogonal to $\boldsymbol{r}_{ik}$ with length $1/|\boldsymbol{r}_{qj}|$ and can be written as

$$\nabla N_j = \frac{\boldsymbol{n}_j}{|\,\boldsymbol{r}_{qj}\,|} = \frac{\boldsymbol{r}_{qj}}{\boldsymbol{r}_{qj}\cdot\boldsymbol{r}_{qj}}. \tag{5}$$

Substituting this expression in (3) and noting that the area of T is given by $A = |\,\boldsymbol{r}_{ln}\,||\,\boldsymbol{r}_{qj}\,|$, we obtain

$$\int_e \nabla N_i \cdot \nabla N_j dE = \nabla N_i \cdot \frac{\boldsymbol{n}_j}{|\,\boldsymbol{r}_{qj}\,|} A = \nabla N_i \cdot \boldsymbol{n}_j |\,\boldsymbol{r}_{ln}\,|.$$

The right-hand side of this equation can be interpreted as the flux of ∇N_i across segment $\overline{ln}$. By the Gauss theorem, this flux can be evaluated as a line integral over any path Γ connecting the edge midpoints l and n; that is,

$$\nabla N_i \cdot \boldsymbol{n}_j |\,\boldsymbol{r}_{ln}\,| = \int_\Gamma \nabla N_i \cdot d\boldsymbol{n}.$$

We have therefore proved the following theorem.

THEOREM 2.1. *Let T be a triangle with vertices i, j, and k, and let N_i and N_j be the linear basis functions associated with nodes i and j, respectively. Then the (ij)th elemental Galerkin stiffness coefficient for equation* (1) *is given by*

$$s_{ij}^{e,G} = \int_\Gamma \nabla N_i \cdot d\boldsymbol{n}, \tag{6}$$

where Γ is the boundary of the nodal control volume of j.

This well-known result (see, e.g., [10]) gives rise to the interpretation of the elemental Galerkin stiffness coefficient as the flux of the basis function gradient across the element nodal control volume. Using simple geometry, we can express $s_{ij}^{e,G}$ as in the following theorem.

THEOREM 2.2. *For the triangle of Theorem* 2.1*, the elemental Galerkin stiffness coefficient between i and j is given by*

$$s_{ij}^{e,G} = \begin{cases} -\dfrac{|\,\boldsymbol{r}_{nc}\,|}{|\,\boldsymbol{r}_{ij}\,|} & \text{if the angle in } k \text{ is} < \frac{\pi}{2}, \\ +\dfrac{|\,\boldsymbol{r}_{nc}\,|}{|\,\boldsymbol{r}_{ij}\,|} & \text{if the angle in } k \text{ is} > \frac{\pi}{2}, \\ 0 & \text{if the angle in } k \text{ is} = \frac{\pi}{2}. \end{cases} \tag{7}$$

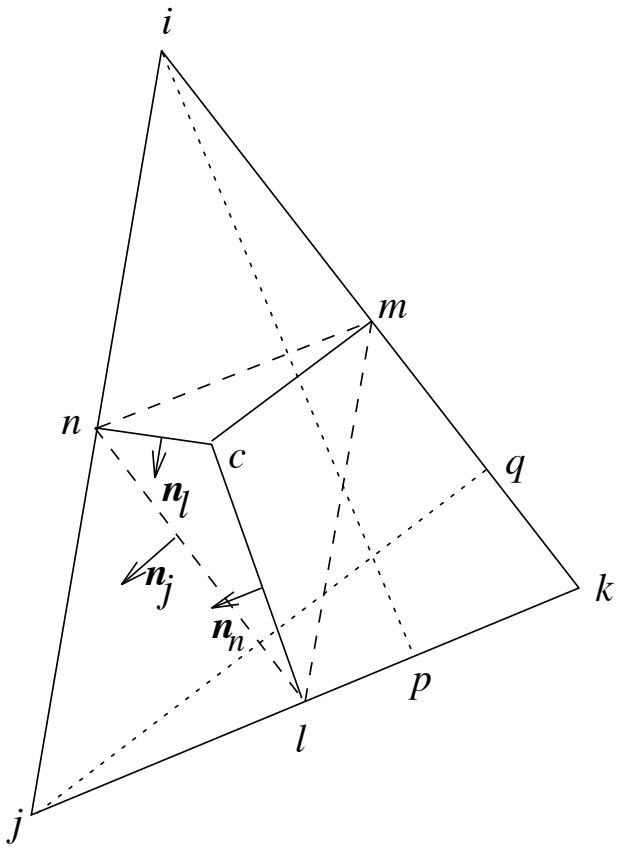

FIG. 2. *Triangular finite element and the corresponding nodal control volumes.*

Proof. Choosing Γ as the Thiessen polygon boundary $\overline{lcn}$ in equation (6) and using (5) we obtain

$$s_{ij}^{e,G} = \frac{\boldsymbol{r}_{pi}}{\boldsymbol{r}_{pi} \cdot \boldsymbol{r}_{pi}} \cdot \left(\int_{nc} d\boldsymbol{n}_l + \int_{cl} d\boldsymbol{n}_n \right).$$

The second integral of this equation gives a null contribution because $\boldsymbol{r}_{pi} \perp \boldsymbol{n}_n$. The first integral can be evaluated as $\mid \boldsymbol{r}_{nc} \mid \boldsymbol{n}_l$. Since $\int_{nc} d\boldsymbol{n}_l = -\int_{cn} d\boldsymbol{n}_l$, its sign changes when the angle in k is $> \frac{\pi}{2}$ (in this case point c lies outside T). Furthermore, if the angle in k is $\frac{\pi}{2}$ then c and n coincide. The proof is completed by noting that $\boldsymbol{n}_l = \boldsymbol{r}_{ij} / \mid \boldsymbol{r}_{ij} \mid$ and that $\boldsymbol{r}_{pi} \cdot \boldsymbol{r}_{ij} = -\boldsymbol{r}_{pi} \cdot \boldsymbol{r}_{pi}$. ∎

The global stiffness coefficient for an interior edge is evaluated as the sum of the elemental stiffness coefficients of two adjacent triangles. From equation (7) it is easy to see that the absolute value of the global stiffness coefficient is equal to the length of the Voronoi cell boundary orthogonal to the common edge (the segment connecting the circumcenters of the two elements), divided by the length of the common edge. The sign has to be found by looking at two adjacent triangles. If the elemental stiffness coefficients of both triangles are negative (e.g., self-centered triangles), then their sum is also negative. For a Delaunay triangulation, if the elemental stiffness coefficient of one of the triangles is positive, the other must be negative. With reference to Figure 3, let T_1 be a non-self-centered triangle. Then $s_{ij}^{T_1,G} = +\mid \boldsymbol{r}_{mc_1} \mid / \mid \boldsymbol{r}_{ij} \mid$,

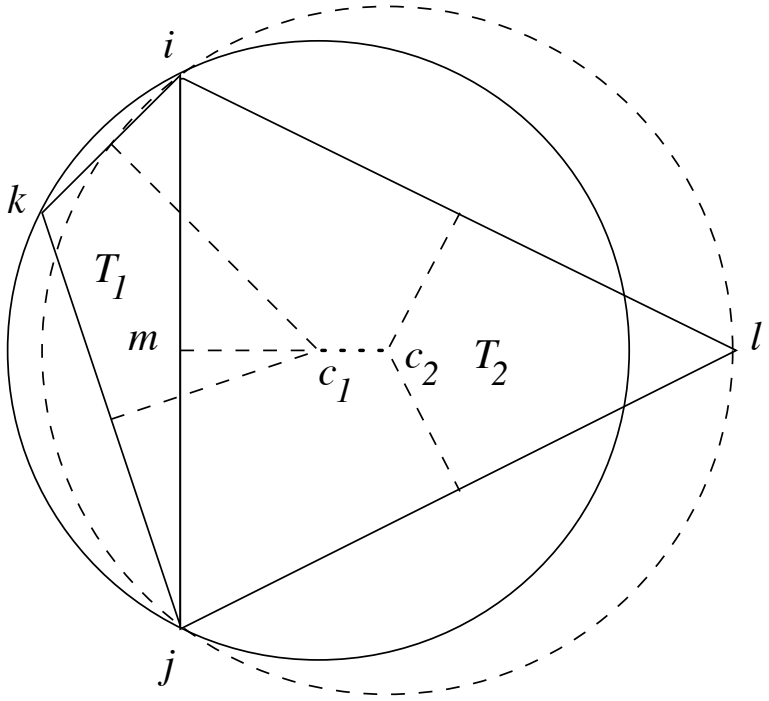

FIG. 3. *Triangular elements in a Delaunay mesh.*

while $s_{ij}^{T_2,G} = -|\,\boldsymbol{r}_{mc_2}\,|/|\,\boldsymbol{r}_{ij}\,|$. Property (P3) ensures that $|\,\boldsymbol{r}_{c_1c_2}\,|$ exists and that $|\,\boldsymbol{r}_{mc_2}\,| \geq |\,\boldsymbol{r}_{mc_1}\,|$. Thus we have the following theorem.

THEOREM 2.3. *In a two-dimensional Delaunay triangulation the global Galerkin stiffness coefficient corresponding to an interior element edge is nonpositive and equal to*

$$s_{ij}^{G} = -\frac{|\,\boldsymbol{r}_{c_1c_2}\,|}{|\,\boldsymbol{r}_{ij}\,|}.$$

This result shows that the PT condition is always satisfied for interior edges of Delaunay meshes. The global stiffness coefficient for an element edge lying on the boundary coincides with the elemental stiffness coefficient and therefore can be positive. However, we can state the following theorem.

THEOREM 2.4. *Let $\mathcal{T}$ be a two-dimensional Delaunay triangulation of a convex domain Ω. If $\mathcal{T}$ satisfies the property that no circumcenters of boundary elements lie outside Ω, and if at least one Dirichlet boundary condition is imposed, then the linear Galerkin finite element method for the discretization of the Laplace operator leads to an M-matrix.*

Proof. An M-matrix S has the properties that $s_{ij} \leq 0$, $s_{ii} > 0$, and $S^{-1} \geq 0$ [11]. If the domain is convex and the circumcenters of all the boundary triangles lie inside the domain, then Theorem 2.2 guarantees that s_{ij}^{G} is nonpositive. From equation (3), it follows directly that $s_{ii}^{G} > 0$, since the area of any triangle in a Delaunay mesh is positive. Finally, the existence of at least one Dirichlet boundary condition implies that the stiffness matrix S is nonsingular. □

If there are boundary elements that do not satisfy the conditions of the previous theorem, it is always possible to change the discretization by defining additional boundary nodes [5].

Remark 2.5. Theorem 2.3 suggests that the Galerkin stiffness equation for the generic node j can be interpreted as a "mass" balance equation on the Voronoi cell of j. Since the union of all the Voronoi cells covers the whole domain Ω, the Galerkin stiffness matrix represents the "mass" balance equation for the entire Ω.

2.2. Three spatial dimensions. As demonstrated by [9], a straight extension of the two-dimensional Galerkin approach to tetrahedra does not lead to a scheme that generally satisfies the PT condition. A better understanding of the linear Galerkin approach can be obtained by analyzing the expression of the stiffness coefficient for the tetrahedron of Figure 4. The four tetrahedron faces can be identified by their normal "area" vectors $\boldsymbol{A}$, directed into the element, given by

$$\begin{aligned} \boldsymbol{A}_i &= \frac{1}{2}\boldsymbol{r}_{jl} \times \boldsymbol{r}_{jk}, \quad \boldsymbol{A}_j = \frac{1}{2}\boldsymbol{r}_{kl} \times \boldsymbol{r}_{ki}, \\ \boldsymbol{A}_k &= \frac{1}{2}\boldsymbol{r}_{il} \times \boldsymbol{r}_{ij}, \quad \boldsymbol{A}_l = \frac{1}{2}\boldsymbol{r}_{ij} \times \boldsymbol{r}_{ik}, \end{aligned} \tag{8}$$

where $\mid \boldsymbol{A}_j \mid$ is the area of face ikl opposite to node j and so on. The gradient of the linear basis function N_j is parallel to vector $\boldsymbol{A}_j$ and can be expressed as

$$\nabla N_j = \frac{\boldsymbol{A}_j}{3V}, \tag{9}$$

where V is the element volume calculated as

$$V = \frac{1}{3}\boldsymbol{A}_j \cdot \boldsymbol{r}_{ij}. \tag{10}$$

Inserting equation (9) into (3), we obtain

$$s_{ij}^{e,G} = \nabla N_i \cdot \frac{\boldsymbol{A}_j}{3}. \tag{11}$$

Thus, $s_{ij}^{e,G}$ can be interpreted as the flux of ∇N_i across a face parallel to the tetrahedron face opposite to node j but having one third of the area. Note that this face intersects the element edges ji, jk, and jl not at the midpoints but at a relative distance of $\sqrt{1/3}$ from node j. The nodal volume individuated by this face cannot be considered as a subdomain as it overlaps with the other nodal volumes of the tetrahedron. Equivalent but nonoverlapping subdomains can be determined by the six faces whose vertices are the six edge midpoints and the gravity centers of the tetrahedron and its four triangular faces. An example of these subdomains is given in Figure 4. As a consequence, Theorem 2.1 can be directly extended to tetrahedral elements when Γ is the boundary of such a nodal subdomain.

For a regular tetrahedron, the centers of gravity of both the tetrahedron and its boundary faces coincide with the respective circumcenters. Then, the six subdomain boundary faces are orthogonal to the element edges and the subdomains correspond to the elemental restrictions of the Voronoi cells. For an irregular tetrahedron there is no such correspondence. As a result, the linear Galerkin stiffness coefficient in three dimensions cannot be defined using the Voronoi mesh, as was done in two dimensions.

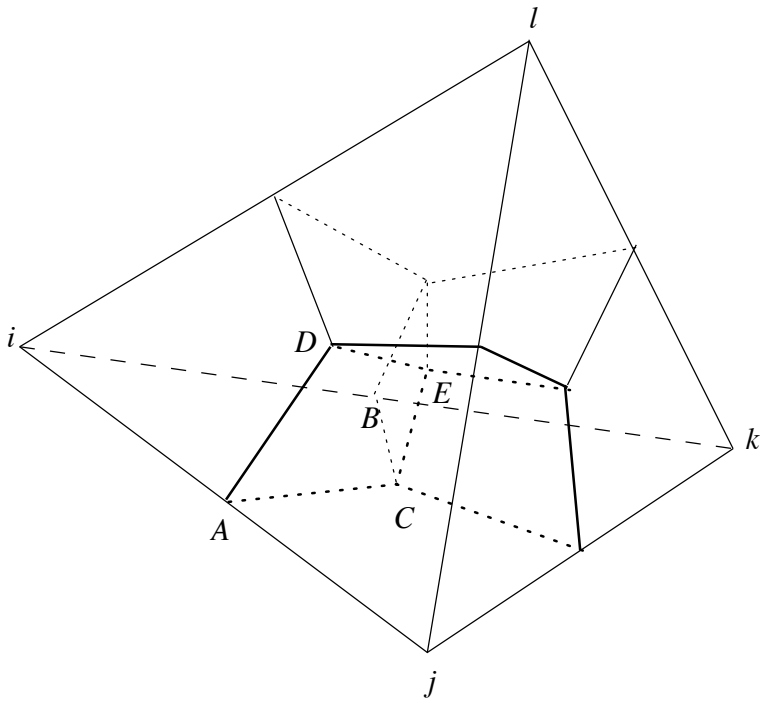

FIG. 4. *Nodal subdomains in a tetrahedral element.*

3. The OSC coefficients. The results of the previous section suggest to modify the linear Galerkin stiffness coefficient by using circumcenters instead of gravity centers as vertices of the corresponding subdomains. This implies the definition of the stiffness coefficient as in equation (6), with the domain of integration Γ being the boundary of the elemental restriction of the Voronoi cell. Thus, this new approach is not based on the Galerkin scheme but rather on a more natural, in this context, subdomain collocation method [15]. The orthogonality of the subdomain faces to the element edges gives rise to the name OSC [2, 3].

The general expression for the OSC elemental stiffness coefficient is derived without loss of generality by focusing on the tetrahedron of Figure 4. Denote by F^e_{ij}, F^e_{kj}, and F^e_{lj} the areas of the three faces perpendicular in the midpoint to the element edges ij, kj, and lj, respectively. The flux of the basis function gradient ∇N_i across the Thiessen polyhedron boundary of node j in element e gives the OSC elemental stiffness coefficient that can be expressed as

$$s_{ij}^{e,OSC} = \nabla N_i \cdot \left(F^e_{ij} \frac{\boldsymbol{r}_{ij}}{|\boldsymbol{r}_{ij}|} + F^e_{kj} \frac{\boldsymbol{r}_{kj}}{|\boldsymbol{r}_{kj}|} + F^e_{lj} \frac{\boldsymbol{r}_{lj}}{|\boldsymbol{r}_{lj}|} \right). \tag{12}$$

Note that this equation constitutes a modification of equation (11) corresponding to the different subdomain geometry. Since ∇N_i is orthogonal to vectors $\boldsymbol{r}_{kj}$ and $\boldsymbol{r}_{lj}$, the last two terms in (12) disappear and only F^e_{ij} contributes to $s_{ij}^{e,OSC}$. Using (9) and (10), and since $\boldsymbol{r}_{ij} = -\boldsymbol{r}_{ji}$, we obtain

$$s_{ij}^{e,OSC} = -\frac{F^e_{ij}}{|\boldsymbol{r}_{ij}|}. \tag{13}$$

This result is a direct extension of Theorem 2.2 to three dimensions, where now the sign is implicitly contained in F_{ij}^e.

The control volume face with area F_{ij}^e has the following points as vertices: A, the edge midpoint; C, the circumcenter of the triangular face ijk; E, the circumcenter of the tetrahedron; and D, the circumcenter of triangle ijl. The calculation of F_{ij}^e proceeds by evaluating the areas of the two triangles ACE and ADE. These can be expressed via the cross products $\frac{1}{2}\boldsymbol{r}_{AC} \times \boldsymbol{r}_{CE}$ and $\frac{1}{2}\boldsymbol{r}_{DE} \times \boldsymbol{r}_{AD}$, respectively. The two resulting vectors are parallel to $\boldsymbol{r}_{ij}$, so the area of the face is obtained by scalar multiplication with the unit vector in this direction:

$$F_{ij}^e = \frac{1}{2}\left(\boldsymbol{r}_{AC} \times \boldsymbol{r}_{CE} + \boldsymbol{r}_{DE} \times \boldsymbol{r}_{AD}\right) \cdot \frac{\boldsymbol{r}_{ij}}{|\,\boldsymbol{r}_{ij}\,|}. \tag{14}$$

Vector $\boldsymbol{r}_{AC}$ is orthogonal to $\boldsymbol{r}_{ij}$ and, since it lies on the plane spanned by nodes i, j, and k, also to $\boldsymbol{A}_l$. Its expression can therefore be written as

$$\boldsymbol{r}_{AC} = \lambda \boldsymbol{r}_{ij} \times \boldsymbol{A}_l, \tag{15}$$

where λ is a scalar factor introduced because the length of $\boldsymbol{r}_{AC}$ is unknown. This length is defined by the identity

$$\frac{1}{2}\boldsymbol{r}_{ij} + \boldsymbol{r}_{AC} = \frac{1}{2}\boldsymbol{r}_{ik} + \boldsymbol{r}_{BC}.$$

Since $\boldsymbol{r}_{BC}$ is orthogonal to $\boldsymbol{r}_{ik}$, it can be eliminated by scalar multiplying both sides of the last equation by $\boldsymbol{r}_{ik}$. Solving for λ and using the expression for $\boldsymbol{A}_l$ in (8) yields the sought expression for $\boldsymbol{r}_{AC}$:

$$\boldsymbol{r}_{AC} = \frac{\boldsymbol{r}_{ik} \cdot \boldsymbol{r}_{jk}}{4\boldsymbol{A}_l \cdot \boldsymbol{A}_l} \boldsymbol{A}_l \times \boldsymbol{r}_{ij}. \tag{16}$$

Vector $\boldsymbol{r}_{AD}$ is obtained in the same way:

$$\boldsymbol{r}_{AD} = \frac{\boldsymbol{r}_{il} \cdot \boldsymbol{r}_{jl}}{4\boldsymbol{A}_k \cdot \boldsymbol{A}_k} \boldsymbol{r}_{ij} \times \boldsymbol{A}_k. \tag{17}$$

Vector $\boldsymbol{r}_{CE}$, being the intersection of the elemental restriction of the Thiessen polyhedra of nodes i, j, and k, is orthogonal to face ijk and can be written as

$$\boldsymbol{r}_{CE} = \gamma \boldsymbol{A}_l, \tag{18}$$

where again γ is a scalar factor introduced because the length of $\boldsymbol{r}_{CE}$ is unknown. As before, consider the identity

$$\boldsymbol{r}_{AC} + \boldsymbol{r}_{CE} = \boldsymbol{r}_{AD} + \boldsymbol{r}_{DE}. \tag{19}$$

Using equations (16), (17), and (18), after scalar multiplication by $\boldsymbol{r}_{AD}$, γ can be explicitly evaluated from equation (19). The expression for $\boldsymbol{r}_{CE}$ is then obtained, after substitution of equations (8) and (10), as

$$\boldsymbol{r}_{CE} = \frac{\boldsymbol{A}_l}{6V}\left[\boldsymbol{r}_{il} \cdot \boldsymbol{r}_{jl} + \boldsymbol{r}_{ik} \cdot \boldsymbol{r}_{jk} \frac{\boldsymbol{A}_k \cdot \boldsymbol{A}_l}{\boldsymbol{A}_l \cdot \boldsymbol{A}_l}\right]. \tag{20}$$

Accordingly, the expression for $\boldsymbol{r}_{DE}$ is

$$\boldsymbol{r}_{DE} = \frac{\boldsymbol{A}_k}{6V}\left[\boldsymbol{r}_{ik} \cdot \boldsymbol{r}_{jk} + \boldsymbol{r}_{il} \cdot \boldsymbol{r}_{jl} \frac{\boldsymbol{A}_k \cdot \boldsymbol{A}_l}{\boldsymbol{A}_k \cdot \boldsymbol{A}_k}\right]. \tag{21}$$

Inserting equations (14), (16), (17), (20), and (21) into (13) and repeating this procedure for the other element edges, the off-diagonal elements of the OSC stiffness matrix are obtained. Their expression is

$$
\begin{aligned}
s_{ij}^{e,OSC} &= -\frac{1}{48V}\left[2(\boldsymbol{r}_{ik}\cdot\boldsymbol{r}_{jk})(\boldsymbol{r}_{il}\cdot\boldsymbol{r}_{jl})+\boldsymbol{A}_k\cdot\boldsymbol{A}_l\left(\frac{(\boldsymbol{r}_{ik}\cdot\boldsymbol{r}_{jk})^2}{\boldsymbol{A}_l\cdot\boldsymbol{A}_l}+\frac{(\boldsymbol{r}_{il}\cdot\boldsymbol{r}_{jl})^2}{\boldsymbol{A}_k\cdot\boldsymbol{A}_k}\right)\right],\\
s_{ik}^{e,OSC} &= -\frac{1}{48V}\left[2(\boldsymbol{r}_{ij}\cdot\boldsymbol{r}_{kj})(\boldsymbol{r}_{il}\cdot\boldsymbol{r}_{kl})+\boldsymbol{A}_j\cdot\boldsymbol{A}_l\left(\frac{(\boldsymbol{r}_{ij}\cdot\boldsymbol{r}_{kj})^2}{\boldsymbol{A}_l\cdot\boldsymbol{A}_l}+\frac{(\boldsymbol{r}_{il}\cdot\boldsymbol{r}_{kl})^2}{\boldsymbol{A}_j\cdot\boldsymbol{A}_j}\right)\right],\\
s_{il}^{e,OSC} &= -\frac{1}{48V}\left[2(\boldsymbol{r}_{ij}\cdot\boldsymbol{r}_{lj})(\boldsymbol{r}_{ik}\cdot\boldsymbol{r}_{lk})+\boldsymbol{A}_j\cdot\boldsymbol{A}_k\left(\frac{(\boldsymbol{r}_{ij}\cdot\boldsymbol{r}_{lj})^2}{\boldsymbol{A}_k\cdot\boldsymbol{A}_k}+\frac{(\boldsymbol{r}_{ik}\cdot\boldsymbol{r}_{lk})^2}{\boldsymbol{A}_j\cdot\boldsymbol{A}_j}\right)\right],\\
s_{jk}^{e,OSC} &= -\frac{1}{48V}\left[2(\boldsymbol{r}_{ji}\cdot\boldsymbol{r}_{ki})(\boldsymbol{r}_{jl}\cdot\boldsymbol{r}_{kl})+\boldsymbol{A}_i\cdot\boldsymbol{A}_l\left(\frac{(\boldsymbol{r}_{ji}\cdot\boldsymbol{r}_{ki})^2}{\boldsymbol{A}_l\cdot\boldsymbol{A}_l}+\frac{(\boldsymbol{r}_{jl}\cdot\boldsymbol{r}_{kl})^2}{\boldsymbol{A}_i\cdot\boldsymbol{A}_i}\right)\right],\\
s_{jl}^{e,OSC} &= -\frac{1}{48V}\left[2(\boldsymbol{r}_{ji}\cdot\boldsymbol{r}_{li})(\boldsymbol{r}_{jk}\cdot\boldsymbol{r}_{lk})+\boldsymbol{A}_i\cdot\boldsymbol{A}_k\left(\frac{(\boldsymbol{r}_{ji}\cdot\boldsymbol{r}_{li})^2}{\boldsymbol{A}_k\cdot\boldsymbol{A}_k}+\frac{(\boldsymbol{r}_{jk}\cdot\boldsymbol{r}_{lk})^2}{\boldsymbol{A}_i\cdot\boldsymbol{A}_i}\right)\right],\\
s_{kl}^{e,OSC} &= -\frac{1}{48V}\left[2(\boldsymbol{r}_{ki}\cdot\boldsymbol{r}_{li})(\boldsymbol{r}_{kj}\cdot\boldsymbol{r}_{lj})+\boldsymbol{A}_i\cdot\boldsymbol{A}_j\left(\frac{(\boldsymbol{r}_{ki}\cdot\boldsymbol{r}_{li})^2}{\boldsymbol{A}_j\cdot\boldsymbol{A}_j}+\frac{(\boldsymbol{r}_{kj}\cdot\boldsymbol{r}_{lj})^2}{\boldsymbol{A}_i\cdot\boldsymbol{A}_i}\right)\right].
\end{aligned}
$$

The diagonal coefficients are calculated using equation (4).

The global stiffness coefficient s_{ij}^{OSC} is given by the sum of all elemental contributions, and therefore it contains the sum of all area contributions $F_{ij}=\sum_e F_{ij}^e$. For an internal element edge ij, F_{ij} is the area of the entire Voronoi cell face orthogonal to ij. Obviously, F_{ij} is nonnegative, since the Voronoi cell face is, by property (P3), bounded and convex. Thus we can state the following theorem.

THEOREM 3.1. *In a three-dimensional Delaunay triangulation the global OSC stiffness coefficient corresponding to an interior element edge is nonpositive and equal to*

$$s_{ij}^{OSC}=-\frac{F_{ij}}{\mid \boldsymbol{r}_{ij}\mid},$$

where F_{ij} is the area of the Voronoi cell boundary orthogonal to edge ij.

If edge ij lies on the boundary, the corresponding Voronoi cell face is unbounded, and we cannot conclude that F_{ij} is nonnegative. However, we can give a sufficient condition for the nonnegativity of F_{ij} in the following theorem.

THEOREM 3.2. *Let $\mathcal{T}$ be a three-dimensional Delaunay triangulation of a convex domain Ω. If $\mathcal{T}$ satisfies the property that no circumcenters of boundary elements and corresponding boundary faces lie outside Ω, and if at least one Dirichlet boundary condition is imposed, then the OSC approach for the discretization of the Laplace operator leads to an M-matrix.*

Proof. What we need to prove is that, for a boundary edge, s_{ij}^{OSC} is negative or zero. The other parts of the theorem follow directly from previous results.

Denote by I the intersection of the domain with the Voronoi cell boundary orthogonal to ij. If no circumcenters of boundary tetrahedra and corresponding boundary faces lie outside Ω, then F_{ij} gives, by construction, the area of I. Since the domain and the Voronoi face are convex, so is I, and therefore $F_{ij}\geq 0$. ∎

Circumcenters of tetrahedra or circumcenters of boundary faces that lie outside Ω do not belong to I. However, they are considered in the calculation of the F_{ij}, which may, in this case, become negative. As in the two-dimensional case, circumcenters outside the domain can be avoided by defining additional boundary nodes.

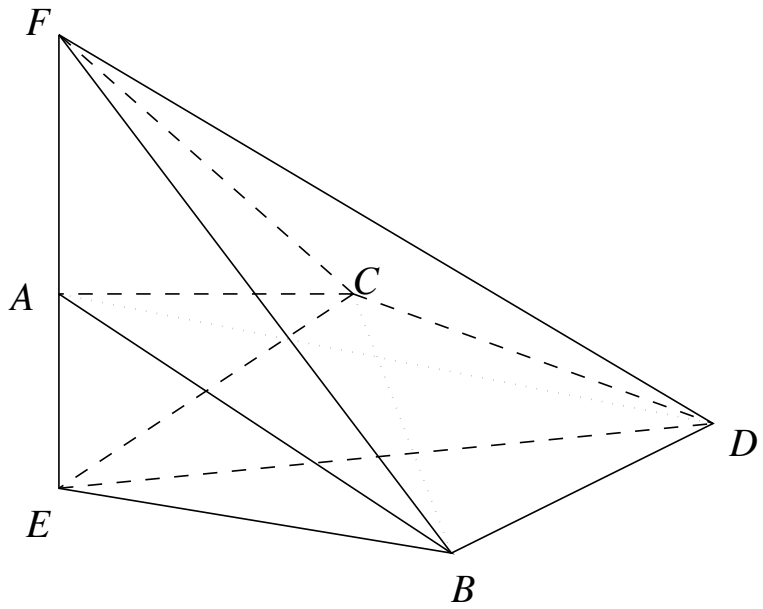

FIG. 5. *Delaunay triangulation used by Letniowski* [9].

4. Numerical examples.

4.1. Letniowski's example with OSC. The OSC approach is first tested on the example that was proposed by [9] to prove that the Galerkin approach cannot guarantee a final M-matrix. This example uses the following six points in space:

$$\begin{array}{rcrrrr} A & = & (& -2, & -2, & 0.5 &), \\ B & = & (& 0, & -2, & 0.1 &), \\ C & = & (& -2, & 0, & 0.1 &), \\ D & = & (& 0, & 0.1, & 0 &), \\ E & = & (& -2, & -2, & -0.25 &), \\ F & = & (& -2, & -2, & 1.5 &). \end{array}$$

There are three possible triangulations of these six points: the first uses AD and BC as internal edges, the second contains only AD, the third contains only BC. The first is the Delaunay triangulation and leads to the five tetrahedra $ABDF$, $ACDF$, $ABCE$, $BCDE$, and $ABCD$ (Figure 5). For all three discretizations, the global Galerkin stiffness coefficient corresponding to the interior connections are positive. In particular, the results for the Delaunay mesh are

$$\begin{aligned} s^G_{AD} &= 2.208, \\ s^G_{BC} &= 3.695. \end{aligned} \tag{22}$$

(As an aside, note that, in Letniowski's paper, the absolute value of s^G_{BC} is different from s^G_{BC} in equation (22); we suppose that the contribution of element $ABCD$ was forgotten.)

Applying the OSC approach to the same five tetrahedra, the global stiffness coefficients for the two inner connections become negative:

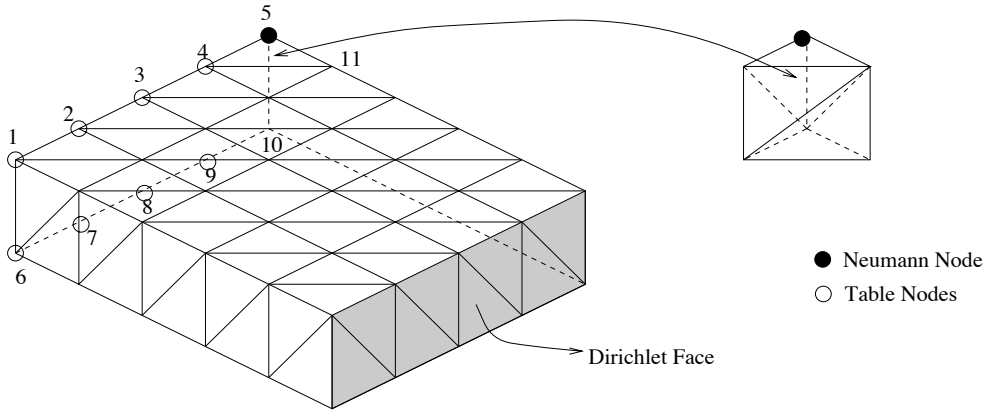

FIG. 6. *Domain and triangulation used in test case* 2.

$$s_{AD}^{OSC} = -0.003287,$$
$$s_{BC}^{OSC} = -0.021680,$$

thus satisfying the PT condition.

4.2. Numerical behavior of OSC. A second example is used to test the practical applicability and the properties of the OSC scheme. The domain and the triangulation employed is schematically shown in Figure 6. The size of the domain is (in dimensionless units) $4 \times 5 \times 1$. Zero Dirichlet boundary conditions are imposed on the shaded area, while all other nodes have no-flow conditions, except the Neumann node (node 5), where a unit source is present.

The mesh shown in Figure 6 has 60 nodes and 120 tetrahedra. From it, four other grid levels are defined by halving each time the sides of the cubic elements. The grids thus defined have 297, 1785, 12,177, and 89,505 nodes, and 960, 7680, 61,440, and 491,520 tetrahedra, for levels 2 to 5, respectively. The tetrahedra are always generated as indicated in the figure [7]. This ensures that the resulting triangulation is Delaunay.

TABLE 1
Comparison of the OSC and Galerkin solutions for test case 2 *on grid level* 4.

	1	2	3	4
	6	7	8	9
Galerkin	0.80885	0.85928	1.0301	1.4587
	0.80982	0.85996	1.0289	1.3826
OSC	0.80936	0.85968	1.0309	1.4615
	0.80935	0.85959	1.0284	1.3832

In Table 1 we report the values of the OSC and Galerkin solution for level 4 at the nodes indicated in Figure 6. According to the flow field imposed, the local gradients should always point toward the Neumann node and therefore should never point downward. From the values in the table we see that the OSC results are consistent with this observation, while the Galerkin ones are not, although the errors are small. These unphysical gradient directions are not restricted to the boundary face of nodes 1-5-10-6 but can be found in a large part of the domain. The Galerkin system matrix

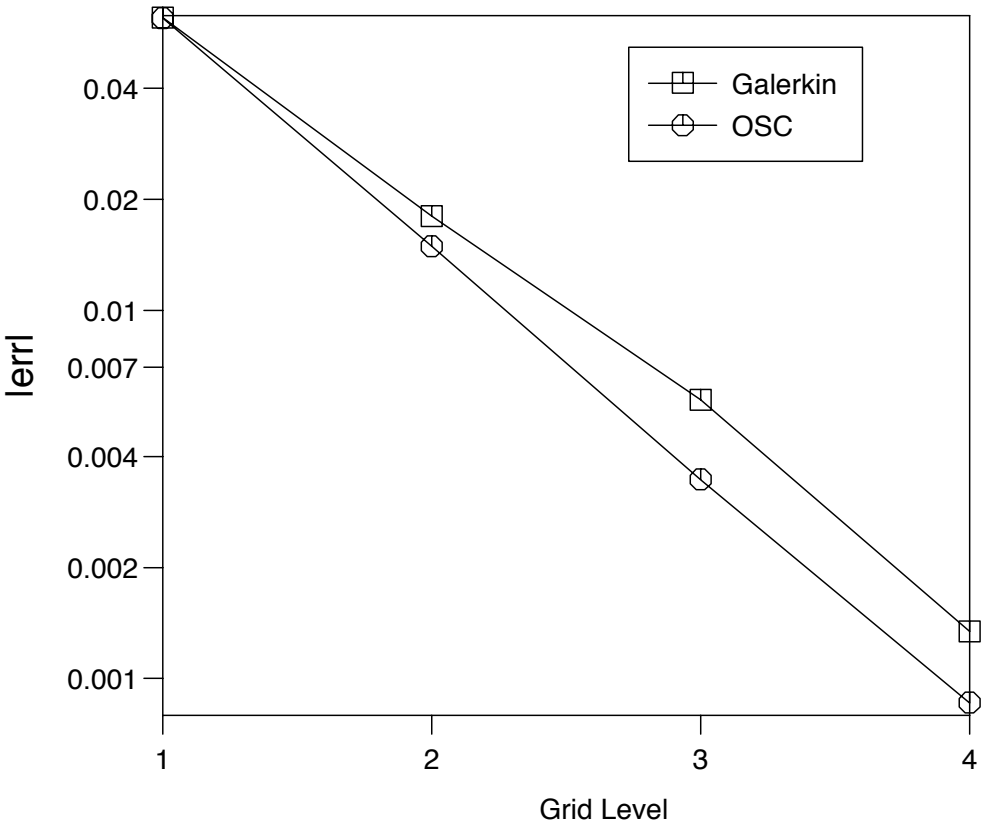

FIG. 7. *Numerical convergence of Galerkin and OSC.*

at grid level 4 has 20,736 positive off-diagonal coefficients (2 per each interior cubic element), while the off-diagonal OSC stiffness coefficients are always nonpositive.

The convergence properties of the OSC approach are evaluated by comparison with the convergence behavior of the Galerkin technique. As the solution to this problem has no simple analytical expression, the Galerkin solution at level 5 is considered as a surrogate analytical solution. The error vectors for both OSC and Galerkin can be defined by taking the difference between the numerical solutions at levels 1 to 4 and the surrogate analytical solution. Note that the presence of a Neumann node introduces a point where the theoretical solution tends to infinity. In this and neighboring nodes, the convergence of the numerical procedures does not reach the asymptotic regime within the five grid refinements. Therefore, the values at nodes 4, 5, 10, and 11 (Figure 6) are neglected, and the error is calculated on the basis of the other 56 nodes of grid level 1. The ℓ_2 norms ($|err|$) of the OSC and Galerkin errors thus obtained are plotted, in a semilogarithmic scale in Figure 7. The plot shows that the behavior of the two schemes is similar and that both schemes tend to the same solution with a quadratic rate of convergence.

The computational efficiency of OSC is similar to that of Galerkin. In the simulation on the finest level, the Galerkin approach was approximately 5% faster than OSC (411 versus 430 seconds on an IBM RS/6000-560) with OSC being slower in the

assembly phase but slightly faster in the solution phase. This last result is explained by noting that the existence of an M-matrix enhances the convergence properties of the preconditioned conjugate gradient scheme that was used in the solution of the linear system.

5. The general diffusion operator. In this section the OSC approach is applied to the general diffusion operator (2) with a possibly nonconstant tensor D. Theorems 2.3 and 2.4 (referring to two-dimensional Galerkin) and Theorems 3.1 and 3.2 (referring to OSC) cannot be extended to a general tensor D. However, it is possible to identify cases where two-dimensional Galerkin and OSC lead to M-matrices [2].

We first consider a variable isotropic D. The tensor in this case reduces to a scalar factor d, which is usually discretized as an elementwise constant function. Positive stiffness coefficients may occur only at interfaces where the elemental d varies (material interfaces). For example, let $d^{(1)}$ and $d^{(2)}$ be the diffusivities of the two elements shown in Figure 3. If $d^{(1)} > d^{(2)}$ then the global Galerkin stiffness coefficient given by

$$s_{ij}^{G} = -\frac{d^{(2)} |\, \boldsymbol{r}_{mc_2} \,| - d^{(1)} |\, \boldsymbol{r}_{mc_1} \,|}{|\boldsymbol{r}_{ij}|}$$

can become positive. These cases do not occur if each of the subsets of the domain where d is constant satisfies the conditions of Theorems 2.4 and 3.2 for two-dimensional Galerkin and OSC, respectively. Otherwise, additional nodes at material interfaces can be introduced, as is done for domain boundaries.

In the case of an anisotropic tensor D, we consider without loss of generality a diagonal tensor with coefficients d_x, d_y, and d_z. In the Galerkin approach D is introduced in the scalar product of the two basis function gradients. In OSC, the replacement of ∇N_i by $D\nabla N_i$ in equation (12) leads to a vector that is not in general orthogonal to edges $\boldsymbol{r}_{kj}$ and $\boldsymbol{r}_{lj}$. To ensure the orthogonality, the original problem is transformed into its isotropic equivalent by distorting the frame of reference [5], i.e., by applying to the nodal coordinates of the element the matrix

$$V = \begin{bmatrix} \sqrt{d/d_x} & 0 & 0 \\ 0 & \sqrt{d/d_y} & 0 \\ 0 & 0 & \sqrt{d/d_z} \end{bmatrix},$$

where $d = \sqrt[3]{d_x d_y d_z}$ is the scalar diffusivity in the distorted system.

If D is constant over the whole domain, distortion can be applied before the Delaunay triangulation is generated. Then Theorems 2.4 and 3.2 hold. If D is variable, an M-matrix is guaranteed only if in each of the subsets of the domain where D is constant the distorted mesh satisfies the conditions of Theorems 2.4 or 3.2.

6. Conclusions. It is well known that it is always possible to find suitable two-dimensional Delaunay triangulations for which the linear Galerkin approach for the discretization of the Laplace operator leads to an M-matrix. However, this cannot be done using tetrahedral meshes. From the interpretation of the Galerkin scheme as a subdomain collocation method, we show that in two dimensions the subdomain faces are orthogonal to the element edges, while this orthogonality is missing in three dimensions (except in the case of a regular tetrahedron). We propose a new method, called OSC, that extends the two-dimensional approach to tetrahedra by keeping the subdomain faces orthogonal to the element edges. Thus, by applying OSC the known properties of the two-dimensional Galerkin scheme can be extended to three

dimensions. In particular, we can prove that under conditions similar to those required in the two-dimensional case the OSC matrix becomes an M-matrix. In a numerical test typical for example of groundwater flow modeling, it is shown that the OSC scheme always preserves the physical correspondence between fluxes and gradients, while the three-dimensional Galerkin approach does not. Finally, we discuss the conditions under which the OSC discretization of a general diffusion operator leads to an M-matrix.

REFERENCES

[1] A. Bowyer, *Computing Dirichlet tessellations*, Comput. J., 24 (1981), pp. 162–166.

[2] C. Cordes, *Bahnkurven in Potentialströmungen*, Ph.D. thesis, Kassel University, Kassel, Germany, 1994.

[3] C. Cordes and W. Kinzelbach, *A subdomain collocation approach in tetrahedral finite elements*, in Computational Methods in Water Resources, Vol. 1, A. Peters, G. Wittum, B. Herrling, U. Meissner, C. A. Brebbia, W. G. Gray, and G. F. Pinder, eds., Kluwer Academic Publishers, Norwell, MA, 1994, pp. 27–34.

[4] H. Edelsbrunner, *Algorithms in Combinatorial Geometry*, Springer-Verlag, Berlin, 1987.

[5] P. A. Forsyth, *A control volume finite element approach to NAPL groundwater contamination*, SIAM J. Sci. Statist. Comput., 12 (1991), pp. 1029–1057.

[6] G. Gambolati, *Diagonally dominant matrices for the finite element method in hydrology*, Internat. J. Numer. Methods Engrg., 6 (1973), pp. 587–591.

[7] G. Gambolati, G. Pini, and T. Tucciarelli, *A 3-D finite element conjugate gradient model of subsurface flow with automatic mesh generation*, Adv. Water Resources, 3 (1986), pp. 34–41.

[8] B. Joe, *Delaunay triangular meshes in convex polygons*, SIAM J. Sci. Statist. Comput., 7 (1986), pp. 514–539.

[9] F. W. Letniowski, *Three-dimensional Delaunay triangulations for finite element approximations to a second-order diffusion operator*, SIAM J. Sci. Statist. Comput., 13 (1992), pp. 765–770.

[10] T. N. Narasimhan and P. A. Witherspoon, *An integrated finite difference method for analyzing fluid flow in porous media*, Water Resour. Res., 12 (1976), pp. 57–64.

[11] J. M. Ortega, *Matrix Theory*, Plenum Press, New York, 1987.

[12] C. Prakash, *Examination of the upwind formulation in the control volume finite element method for fluid flow and heat transfer*, Numer. Heat Transfer, 11 (1987), pp. 401–416.

[13] J. Risler, *Mathematical Methods for CAD*, Cambridge University Press, Cambridge, MA, 1992.

[14] G. E. Schneider and M. J. Raw, *A skewed, positive influence coefficient upwinding procedure for control volume based finite element convection diffusion computation*, Numer. Heat Transfer, 9 (1986), pp. 1–26.

[15] O. C. Zienkiewicz, *The Finite Element Method*, McGraw–Hill, New York, 1986.